AeroBest 2025
Lisboa, 22–24 April 2025
©ECCOMAS, Portugal

# HIGH ASPECT-RATIO COMPOSITE WING AEROSTRUCTURAL OPTIMISATION OF A SHORT-MEDIUM RANGE AIRCRAFT

**Luís M. M. Pacheco[1,2*], Fabian Volle[3], Ögmundur Petersson[2] and André C. Marta[1*]**

1:IDMEC
Instituto Superior Técnico, Universidade de Lisboa
Av. Rovisco Pais, 1, 1049-001 Lisboa, Portugal
* {luis.miguel.martins.pacheco, andre.marta}@tecnico.ulisboa.pt,
https://mdo.tecnico.ulisboa.pt

2: Airbus Defence and Space
Department of Stress Methods and Optimisation
Rechliner Straße, 85077, Manching, Germany

3: DLR
Institute of Aerodynamics and Flow Technology
Lilienthalplatz 7, 38108, Braunschweig, Germany

**Abstract.** *A key pathway towards climate-neutral aviation lies in the adoption of high aspect-ratio wings, which reduce lift-induced drag. A recently developed high-fidelity multidisciplinary design optimisation framework, incorporating DLR's aerodynamic TAU solver and Airbus' structural Lagrange solver, is used for the aeroelastic structural sizing optimisation of two high aspect-ratio composite medium-range transport aircraft wings. Three distinct objective functions are considered: i) the classical minimisation of mass, ii) the maximisation of aerodynamic efficiency, and iii) the maximisation of Breguet range. A gradient-based algorithm with direct sensitivity analysis is used. The design variables include structural sizing parameters such as the thickness or cross-sectional area of the skin, spars, and stringers. Constraints reflect industry requirements, encompassing structural strength, buckling stability, and manufacturing criteria. For the objective functions and design points analysed, the findings highlight the advantages of high aspect-ratio wings in reducing drag and improving aerodynamic efficiency, despite the increase in structural weight. Optimising for Breguet range results in a trade-off between structural and aerodynamic efficiency, demonstrating the benefits of considering a multidisciplinary performance-based objective for structural sizing in the preliminary design phase.*

**Keywords:** Multidisciplinary Design Optimisation, Structural Sizing, Composite High Aspect-Ratio Wings, Breguet Range, Aerodynamic Efficiency

## 1 INTRODUCTION

The environmental impact of the aviation industry has become an increasingly pressing concern, particularly in the context of climate change. This problem is poised to intensify, as the current pace of technological advancements fails to offset the rise in emissions caused by air traffic growth [1]. To address this challenge, the development of novel, environmentally sustainable aircraft configurations is imperative.

Among various proposed designs, increasing the aspect ratio (AR) of wings has emerged as a particularly effective concept to improve aircraft efficiency. This reduces induced drag, which accounts for about 40% of total drag in cruise for transport aircraft [2]. However, it comes with a structural weight penalty due to higher wing root bending moments.

This gives rise to a tightly coupled and conflicting set of design objectives across the aerodynamic and structural domains. As such, a multidisciplinary design optimisation (MDO) approach becomes essential to explore these inherent trade-offs in a highly automated manner and identify the optimal balance between AR and structural integrity that maximises performance.

These trade-offs have been explored with a combined shape parameter study and sizing optimisation of a composite-wing UAV [3] to determine the optimal aspect ratio and structural sizing for maximum range. Five UAV variants, with aspect ratios ranging from 12 to 24, were structurally sized using a gradient-based aeroelastic optimisation. The results indicated that an aspect ratio of 16.8 was optimal, highlighting the fact that the performance benefits of reducing induced drag by increasing aspect ratio are eventually offset by the additional mass required to satisfy structural constraints.

The influence of metallic and composite materials, as well as the choice of objective function, on the trade-off between weight and drag has also been investigated [4], using gradient-based aerostructural optimisations considering aerodynamic shape and structural sizing, with strength and buckling constraints. The resulting Pareto front of fuel burn and take-off gross weight showed distinct optimal planforms, with fuel burn minimisation favouring higher aspect ratios and span. Furthermore, composite wings were found to be up to 40% lighter, resulting in fuel burn savings of up to 8%. These findings highlight the benefits of using composite materials for greener aircraft.

The present study pursues a twofold objective. Firstly, it aims to investigate the impact of increasing the aspect ratio on the performance of a transport aircraft. To this end, two variants of the DLR-F25 [5, 6] with different aspect ratios were structurally sized using a gradient-based algorithm with direct sensitivity analysis. The optimisations considered strength, buckling, and manufacturing constraints, reflecting industry requirements. Secondly, the influence of different objective functions on the structural sizing is explored, namely: minimisation of weight, maximisation of lift-to-drag ratio, and maximisation of the Breguet range. The objective is not only to compare the final designs but also to assess whether the use of computational fluid dynamics (CFD), necessary to compute the latter two objectives, is justified during the preliminary design stage.

The remainder of this paper is structured as follows: first, a brief description of the aerostructural optimisation process and disciplines is done. Subsequently, both DLR-F25 variants and the analysis models used in this study, are introduced. The results of the structural sizing for the different objective functions are then presented, followed by a discussion of the impact of AR and objective function on overall performance. Finally, the conclusions of the study are drawn, and suggestions for future research are provided.

## 2 METHODOLOGY

Three distinct objectives are proposed for the structural sizing optimisations: i) the classical minimisation of mass, ii) the maximisation of lift-to-drag ratio, and iii) the maximisation of Breguet range. In all optimisations, an aerostructural analysis based on linear aerodynamics is used to determine the loads for the structural sizing. Potential flow methods are chosen due to their sufficient accuracy in lift load distribution estimates in the preliminary design stage at a relatively low computational cost [7]. Moreover, they exhibit robustness to the large wingtip displacements induced by structurally critical loads, a feature often lacking in higher-fidelity models.

While the mass objective can be directly obtained from the structural model during the structural sizing process without the need for additional calculations, the other two objectives require additional computations to estimate drag. Since drag can only be reliably predicted with high-fidelity aerodynamics, a distinct aerostructural analysis model from that used to drive the structural sizing is required in these cases.

As a result, two distinct optimisation processes are put in place, whose XDSM diagrams [8] are presented in Figures 1 and 2. The first focuses on the mass objective and relies exclusively on the linear aerostructural analysis, while the second addresses the drag-dependent objectives by incorporating an additional expensive high-fidelity aerostructural analysis.

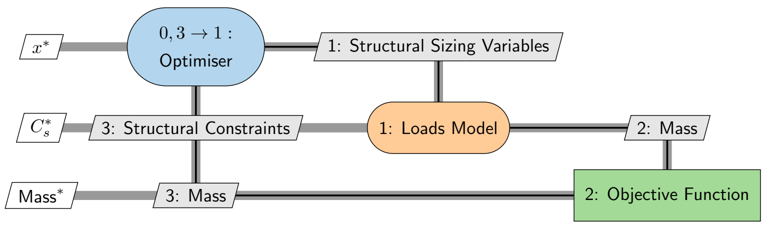


Figure 1: Structural sizing optimisation process for mass minimisation.

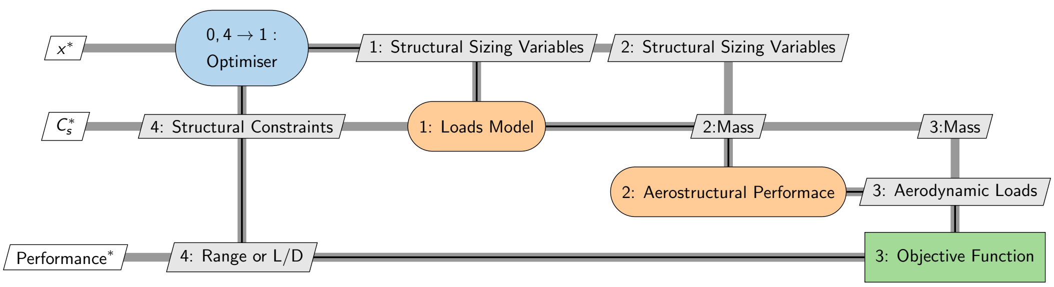


Figure 2: Structural sizing optimisation process for lift-to-drag or Breguet range maximisation.

All optimisations are conducted using a high-fidelity multidisciplinary design optimisation framework [9–11]. This framework couples Airbus's in-house MDO suite, Lagrange [12, 13], with DLR's flow solver, TAU [14, 15], through the high-performance computing software integration platform, FlowSimulator [16].

These two aerostructural design processes include two major analysis modules: the loads model (1), which directly drives the structural sizing, and the higher-fidelity counterpart (2), needed to evaluate the drag-dependent objective functions, described next.

## 2.1 Loads Model

The aerostructural coupling is handled in the form of a multidisicplinary analysis (MDA), posed as an iterative process that includes the fluid flow solution, load interpolation, structural deformation, and displacement transfer, as illustrated in Figure 3.

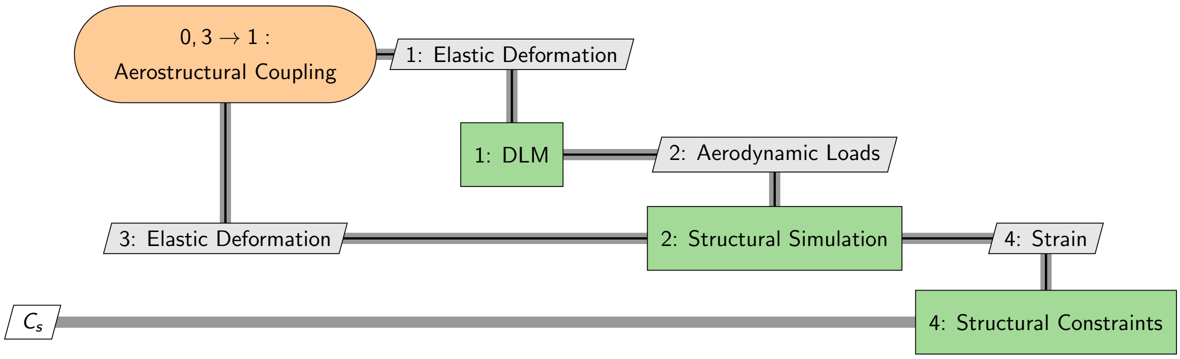


Figure 3: Coupled aerostructural analysis driving the loads model.

The process starts with the linear aerodynamic solution. The resulting loads are interpolated to the structural model using the infinite plate spline method, outlined in Section 2.5. Using these aerodynamic forces and adding the inertial loads, the structural problem is solved, yielding the elastic displacement field. These structural deformations are applied to the aerodynamic model, altering the lift distribution on the wing and starting over the iterative loop. After the coupling has converged, the structural constraints are evaluated.

## 2.2 Aerostructural Performance

The high-fidelity aerostructural analysis needed to evaluate the drag-dependent objective functions is based on a three-field formulation of the coupled aerostructural problem, where the mesh deformation is incorporated as an additional discipline alongside aerodynamic and structural analysis, as illustrated in Figure 4.

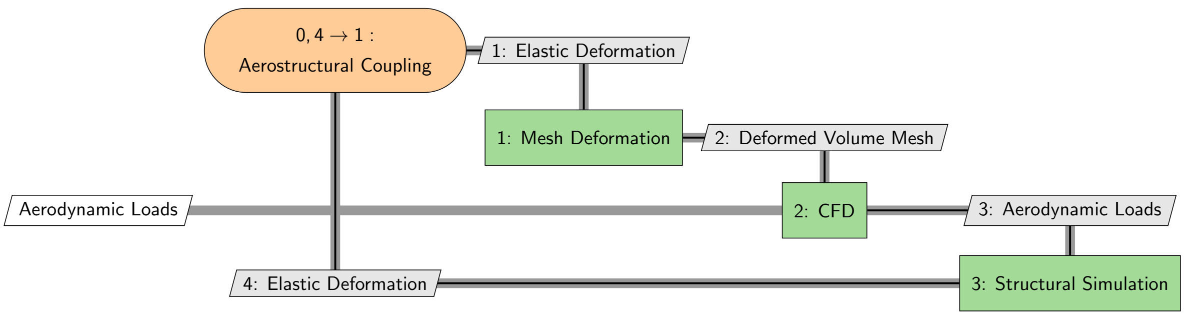


Figure 4: Coupled aerostructural analysis for the drag-dependent objective functions.

The analysis begins with a CFD simulation, solving the governing flow equations. The aerodynamic forces are then interpolated from the aerodynamic domain onto the structural mesh using the moving least squares method, outlined in Section 2.5. Considering these aerodynamic forces and the inertial loads, the structural deformations are computed and interpolated onto the aerodynamic surface mesh. These deformations are applied as boundary conditions in the mesh deformation problem, which is solved using a linear elasticity analogy method, presented in Section 2.6. The outcome of this aerostructural analysis is the aerodynamic loads used to compute the lift-to-drag and Breguet range objective functions.

The convergence criterion of this coupling process is defined by the $L^2$ norm of the variation in elastic deformation at the fluid-solid interface. The rate of convergence for the aerostructural coupling is improved through a dynamic under-relaxation technique using the standard Aitken $\Delta^2$ method [17].

These two processes share the same structural model but use different aerodynamic models, as described next.

### 2.3 Structural Model

In both processes, the structural problem is governed by Hooke's law of elasticity. The structural residuum $R_S$ can be expressed as

$$\mathcal{R}_S = K y_S - F_S = 0\,, \tag{1}$$

where $K$ is the symmetric stiffness matrix, $y_S$ is the state variables vector representing the structural displacements, and $F_S$ is the sum of aerodynamic and inertia forces acting on the aircraft. The structural problem is solved using the built-in finite element solver of Airbus's MDO suite Lagrange [12, 13].

### 2.4 Aerodynamic Models

Two levels of fidelity are used for the aerodynamic discipline: high-fidelity aerodynamics is used to calculate the loads needed to evaluate the drag-dependent objective functions, whereas a low-fidelity linear aerodynamic model is used for the structural sizing process.

The linear aerodynamic model is the doublet lattice method (DLM) [18]. In this method, the aerodynamic system is solved once in advance to generate the complex-valued aerodynamic influence coefficient (AIC) matrix. This matrix is then provided to Lagrange, which incorporates a linear aerodynamic analysis tool capable of computing the aerodynamic loads acting on the structure [12].

In the high-fidelity model, the fluid problem is governed by the compressible Reynolds-averaged Navier-Stokes (RANS) equations, coupled with the Spalart-Allmaras (SA) one equation turbulence model in its negative formulation. In differential form, the residuals of the flow governing equations are expressed as

$$\mathcal{R}_F = \frac{\partial y_F}{\partial t} + \nabla \cdot (\phi_c - \phi_v) = 0\,, \tag{2}$$

where $\phi_c$ and $\phi_v$ are the convective and diffusive fluxes, respectively, and the state variables $y_F$ denote the conserved quantities of the flow. These equations are discretised with the finite volume method and solved using DLR's CFD solver TAU [14, 15].

### 2.5 Loads And Displacement Transfer

Due to the distinct domain discretisations, the meshes at the fluid-structure interface typically do not match, preventing direct information exchange.

For the aerostructural analysis of the loads model, aerodynamic loads and elastic displacements are interpolated through a set of structural nodes using the infinite plate spline (IPS) method [19]. For the aerostructural analysis used to calculate the drag-dependent objectives, a mesh-free approach based on the moving least squares (MLS) method [20] is used. This method to transfer forces and displacements between the structural and aerodynamic boundary meshes is both conservative and consistent.

### 2.6 Aerodynamic Mesh Deformation

When the DLM method is used in the loads model, no volume mesh deformation is required. In contrast, the aerostructural analysis used to calculate the drag-dependent objectives requires that the aerodynamic volume mesh must adapt to the deformation of its surface mesh induced by the structural displacement. The mesh deformation method used is based on the linear elasticity analogy [21], whereby the fluid flow mesh is considered analogous to a volumetric structure problem. The governing equation for the mesh deformation problem is given by

$$\mathcal{R}_M = K_M y_M - F_M(u) = 0\,, \tag{3}$$

where $K_M$ is a symmetric stiffness matrix constructed by assigning stiffnesses to each element of the fluid flow mesh, inversely proportional to the element's volume, and $F_M$ is a fictitious force imposing the Dirichlet boundary condition of the structural displacements at the aerodynamic surface mesh.

## 3 DLR-F25 MODELS

In order to investigate the impact of increasing the aspect ratio on aircraft performance, two aircraft models were structurally sized: the high aspect-ratio DLR-F25 and a newly developed variant with an even greater aspect ratio.

### 3.1 Baseline Geometric Model

The DLR-F25 is a single-aisle, narrow-body aircraft model with a high aspect-ratio wing, designed for the short-to-medium range market segment [5, 6]. It has been primarily developed by the DLR and it is based on the Airbus A321neo. This research aircraft model is currently used in the UPWing project [22] as a reference platform for assessing and validating innovative technologies.

The baseline DLR-F25 wing planform is divided by five sections - centre, root, kink, mid, and tip - as depicted in Figure 5.

The key characteristics of the baseline DLR-F25 wing are summarised in Table 1. Its aspect ratio of 15.6 is significantly higher than that of conventional transport aircraft, such as the Airbus A321-100, which has an aspect ratio of 9.4 [23]. The DLR-F25 wing has a tip chord of 0.6 metres and a taper ratio of 0.12, resulting in a considerably thinner and narrower wing compared to a typical transport aircraft, such as those of the Airbus A320 family, whose tip chord measures approximately 1.5 metres and have taper ratios of 0.24 [23, 24].

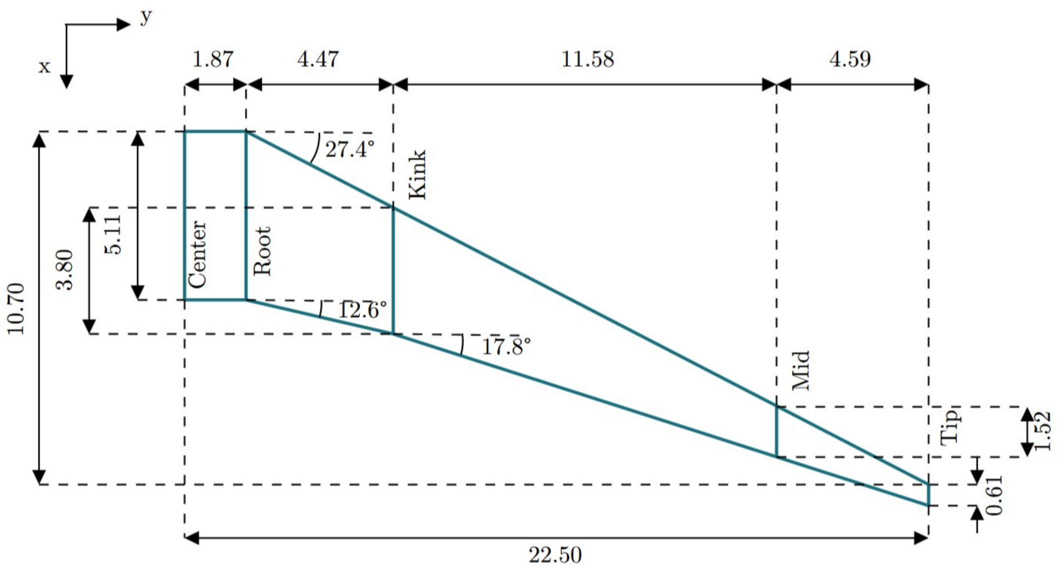


Figure 5: DLR-F25 wing planform (dimensions in metres) [6].

The DLR-F25 features a carry-through wingbox extending through the fuselage. The wing comprises a two-spar design with 31 ribs per half-span and 11 stringers, which progressively taper as the wing narrows towards the tip. The ribs and stringers have a minimum pitch of 800 mm and 220 mm, respectively, to prevent buckling from becoming a dominant design constraint.

### 3.2 Higher Aspect-Ratio Variant Geometric Model

The DLR-F25 baseline aircraft was modelled using a parametric geometry representation in CPACS [25, 26], wherein the positions of structural components were defined relative to the wing's coordinate system. This approach enables the automatic adjustment of component positions in response to shape variations, such as an increase in wingspan.

Leveraging that parametric geometry, a higher aspect-ratio variant of the DLR-F25 was generated by modifying the baseline wing shape using Airbus's in-house tool Descartes [27, 28]. Descartes is a pre-processing tool capable of generating a parametric geometry model, from which it can derive the necessary input data for structural sizing, including structural and aerodynamic models, as well as the optimisation model itself.

In the higher aspect-ratio variant, it was decided that the central part of the wing, up to the kink section, remained unaltered to preserve the wing-fuselage junction and the original pylon attachment configuration. Consequently, only the outer wing sections, aft of the engine position, were modified.

Several methods exist in the literature for increasing an aircraft's aspect ratio, involving changing or preserving parameters such as taper ratio, trailing and leading-edge sweep, or wing surface area, depending on the design objectives [6]. Some of these methods are illustrated in Figure 6.

For this study, the area method depicted in Figure 6b was adopted. This method maintains the leading-edge sweep and taper ratio constant but increases the surface area and trailing-edge sweep. This approach was selected to prevent unintended aerodynamic effects that could arise from varying the taper ratio, which might obscure or counteract the impact of increasing the aspect ratio. Maintaining the baseline taper ratio was particularly

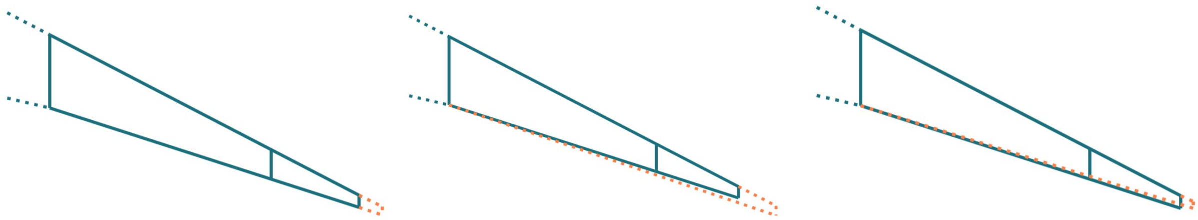

(a) Span variation. (b) Area variation. (c) Tip chord variation.

Figure 6: Schematic representation of different aspect-ratio variation methods [6].

critical, given that the DLR-F25's taper ratio was already small, and further reduction would pose significant aerodynamic challenges at the wingtip. Furthermore, this method has been shown to provide a longitudinally stable aircraft [6] and, among the methods shown in Figure 6, it is the most effective in reducing induced drag.

Using this approach, the new higher aspect-ratio DLR-F25 variant was generated in Descartes by stretching the baseline´s outer wing segments, increasing the overall wingspan by 10%. This resulted in a new aircraft model with a 11.5% higher aspect ratio of 17.4 and a 7.5% larger wing surface area. The vertical and horizontal tailplanes remained unchanged and the maximum take-off weight was considered a top-level aircraft requirement and, therefore, kept constant. Henceforth, the baseline DLR-F25 and its higher aspect-ratio variant will be referred to as F25-AR15 and F25-AR17, respectively. Table 1 summarises the main geometrical differences between the model's wings.

Table 1: DLR-F25 wing key characteristics: baseline and higher aspect-ratio wings.

| **Parameter** | | **F25-AR15** | **F25-AR17** |
|---|---|---|---|
| Aspect ratio | $AR$ | 15.6 | 17.4 |
| Wingspan | $b$ | 44.60 m | 49.04 m |
| Wing area | $S$ | 129.59 m$^2$ | 139.21 m$^2$ |
| Sweep at $\frac{1}{4}$ chord | $\Lambda_{c/4}$ | 24.43° | 24.69° |
| Taper ratio | $\lambda$ | 0.12 | 0.12 |

The substantial increase in aspect ratio for the F25-AR17 altered the baseline rib pitch. This resulted in significantly larger buckling fields for the F25-AR17, making buckling a critical design constraint and precluding a fair direct comparison between the two aspect ratio variants. Consequently a topological modification to the F25-AR17 wing structure was performed, where two additional ribs were incorporated into the middle section of the wing and one near its tip.

### 3.3 Structural Analysis Models

The finite element (FE) structural models were generated using Descartes' internal meshing functionality. The skins, spars, and ribs, were modelled using shell elements, specifically CQUAD4 and CTRIA3, whilst the stringers and spar caps were represented using one-dimensional elements, namely CBAR and CROD, respectively. The FE structural model for the F25-AR15 is depicted in Figure 7.

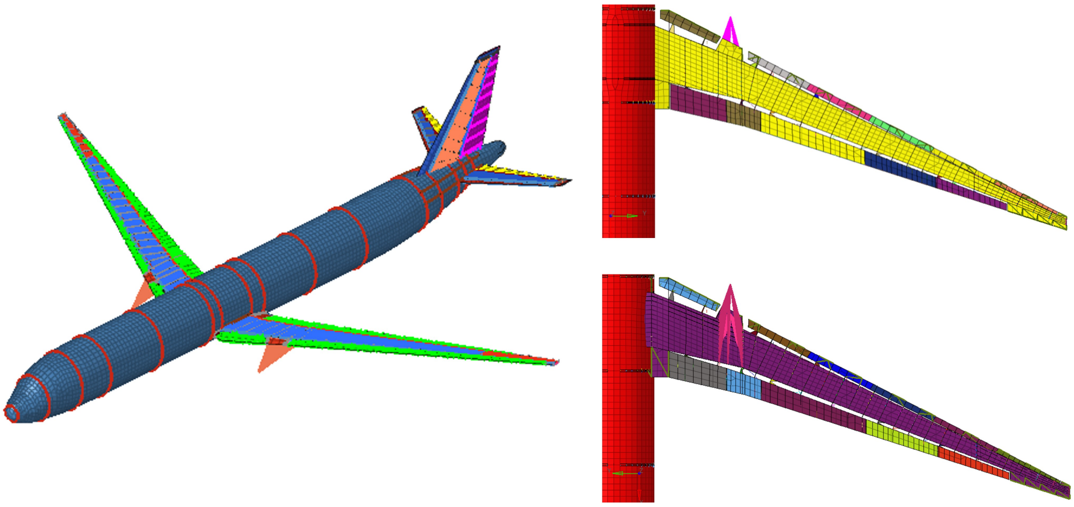

Figure 7: FE structural model of the F25-AR15 variant.

The F25-AR17 model follows a comparable discretisation approach, as both models were constructed using the same methodology. Table 2 presents a comparative summary of the refinement and discretisation used in the structural modelling of each aircraft variant.

Table 2: Structural discretization and elements of F25-AR15 and F25-AR17 wings.

| **Parameter** | **F25-AR15** | **F25-AR17** |
|---|---|---|
| Nodes | 13,152 | 13,331 |
| CQUAD4 elements | 13,567 | 13,815 |
| CTRIA3 elements | 1,191 | 1,201 |
| CROD elements | 5,812 | 5,906 |
| CBAR elements | 3,175 | 3,331 |

The DLR-F25 model considers two distinct mass configurations: the maximum take-off weight (MTOW) of 81,656 kg and the maximum zero fuel weight (MZFW) of 69,322 kg. The MTOW configuration serves as the driver for structural sizing, whereas the MZFW configuration is used to determine the aerodynamic loads required for the drag-dependent objective functions. Irrespective of the mass configuration, the aircraft weight is divided into two components: the structural weight of the composite wing and the combined weight of the fuel, payload, passengers, and the remaining aircraft structure, including engines and pylons.

The weight of the composite wing is evaluated from the size and material properties of its finite elements. The wing skin and spar webs are modelled using a symmetric and balanced 24-ply carbon fibre reinforced polymer (CFRP) laminate with four ply orientations (0°, 90°, and ±45°), and a material density of 1580 kg/m$^3$. The T-shaped stringers and spar caps are modelled using homogenised CFRP properties, assuming a ply distribution of 70% at 0°, 20% at ±45°, and 10% at 90°, with a density of 1750 kg/m$^3$.

The remaining weight is represented by 131 distributed concentrated mass points, implemented as CONM2 elements and connected to the FE model via rigid body elements

(RBE), as illustrated in Figure 8.

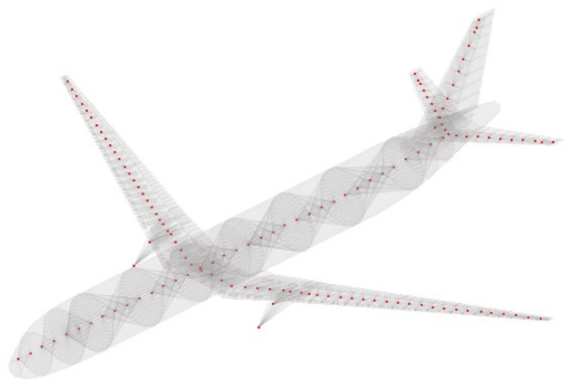

Figure 8: F25-AR15 CONM2 mass point distribution.

### 3.4 Aerodynamic Models

As detailed in Section 2.4, this study employs two levels of fidelity for the aerodynamic discipline. High-fidelity aerodynamics is used for the evaluation of objective functions, whereas the structural sizing optimisation relies on a linear aerodynamic model.

The DLM meshes used in the loads model were generated from the parameterised geometric models using Descartes. The entire aircraft, including the wing, fuselage, and vertical and horizontal tailplanes, was discretised, as presented in Figure 9a for the F25-AR15. The wing was discretised into 7 panels in the chordwise direction and 43 panels in the spanwise direction. The discretisation for the F25-AR17 follows the same approach.

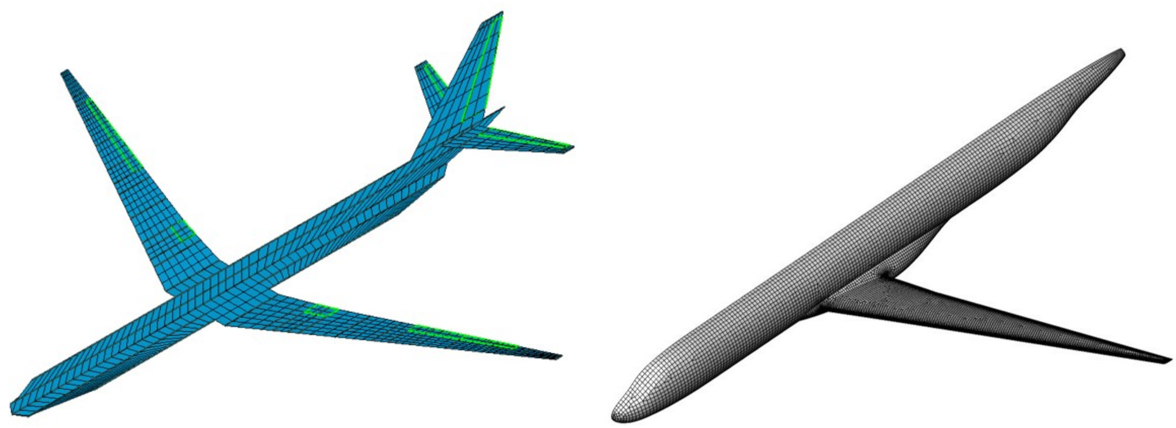

(a) Doublet lattice method mesh. (b) High-fidelity aerodynamic surface mesh.

Figure 9: F25-AR15 aerodynamic mesh.

The high-fidelity aerodynamic mesh used in the aerostructural performance analysis, is based on a wing-body configuration of the DLR-F25. To reduce the computational cost associated with CFD analyses, a half-model of the aircraft is used, leveraging the symmetry of the configuration, as illustrated in Figure 9b for the F25-AR15. This computational grid, comprising 1.02 million nodes, was developed by DLR. The aerodynamic model of the F25-AR17 was generated by morphing the existing F25-AR15 mesh, therefore both meshes are topologically identical with the same number of nodes and elements.

### 3.5 Coupling Models

The IPS method used in the aerostructural analysis of the loads model requires a set of nodes. These nodes are strategically arranged in a diamond pattern at the intersections of the wing's upper skin with the spars and ribs. Beyond the wingbox, this approach is extended to the fuselage and the horizontal and vertical tailplanes. Figure 10 illustrates the nodal distribution for the F25-AR15 wing. The coupling model for the F25-AR17 follows the same principles.

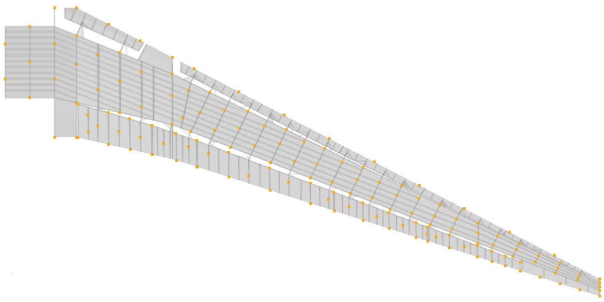

Figure 10: F25-AR15 wing coupling for the loads model.

In the aerostructural analysis used to compute the drag-dependent objectives, the MLS method was used, which does not rely on a predefined set of nodes.

### 3.6 Optimisation Problem

The three proposed objectives for the structural sizing optimisations are the minimisation of the wingbox mass, and the maximisation of lift-to-drag ratio and Breguet range.

All optimisations are performed using the gradient-based NLPQL optimisation algorithm [29] with a direct sensitivity analysis. The optimisations converge based on a Karush-Kuhn-Tucker (KKT) criterion [30] of $10^{-5}$. An active-set strategy is implemented, restricting the sensitivity analysis to the 20,000 most violated constraints.

The optimisation focused exclusively on the structural sizing of the composite wingbox, specifically the skin, spars, and stringers. The design variables are defined within patches. For the skin, each patch is bounded by two ribs and two stringers, whereas patches for the stringers and spars are segmented by ribs. These patches are symmetrically linked to ensure both sides of the wing were identical. Within each skin and spar web patch, plies of the same orientation are linked to preserve laminate symmetry. To ensure a balanced laminate, the thicknesses of the $+45°$ and $-45°$ plies are also linked. Consequently, three independent design variables per skin and spar web patch control the thickness of the ply orientations. Each spar cap patch is governed by a single design variable that determines its cross-sectional area. The T-shaped stringers are characterised by three design variables, which define the web height, foot width and thickness. The thickness of the foot and web are linked in a 1:2 ratio. The bounds and initial values for the design variables are presented in Table 3.

The structural sizing criteria for the composite wing focus primarily on optimising the wing covers, as they are the main driver for aeroelastic tailoring. Constraints on strength,

Table 3: Design variables and their bounds for structural sizing.

| Component | Section | Design Variable | Lower Bound | Initial Value | Upper Bound |
|---|---|---|---|---|---|
| Skin | Upper skin | Ply thickness [mm] | 0.164 | 0.254 | 2 |
| | Lower skin root | | 0.254 | 0.508 | 2 |
| | Lower skin kink | | 0.254 | 1.016 | 2.5 |
| | Lower skin tip | | 0.254 | 0.381 | 2 |
| Spar | Inner & outer | Web ply thickness [mm] | 0.164 | 0.254 | 2 |
| | | Cap area [mm$^2$] | 80 | 100 | 1000 |
| Stringer | Inner | Web height [mm] | 51.5 | 66.5 | 81.5 |
| | | Foot length [mm] | 80 | 100 | 120 |
| | | Foot thickness [mm] | 3 | 3 | 9 |
| | Outer | Web height [mm] | 51.5 | 66.5 | 68.5 |
| | | Foot length [mm] | 80 | 100 | 120 |
| | | Foot thickness [mm] | 3 | 3 | 6 |

buckling, and manufacturability are incorporated into the sizing optimisations. Strength constraints are uniformly applied to the skin, spars, and stringers, with maximum allowable material strains of 5000 $\mu\varepsilon$ in tension and 3500 $\mu\varepsilon$ in compression and a safety factor of 1.5 incorporated. The skin and spar buckling panels are modelled as biaxially loaded, simply supported flat plates with anisotropic material properties. The critical buckling loads are determined using analytical methods [31–33]. Stringer buckling is evaluated by modelling the stringer and attached sheet as a super-stiffener, with the critical buckling strength determined via the Johnson-Euler formula [34]. A correction factor of 0.95 is applied to the skin buckling field size to account for the idealised representation of the stringers as one-dimensional elements. To ensure manufacturability, thickness and ply share constraints are imposed. Thickness variations between adjacent skin patches are limited by a ramp rate of 1:20 in the spanwise direction and 1:10 in the chordwise direction. Additionally, continuity constraints prevent abrupt ply share variations by restricting thickness differences between adjacent plies to 1/10 of the ply thickness. Ply share percentages in the skin are constrained to a range of 10 to 63% for 0° and 90° plies and 20 to 80% for ±45° plies. Additionally, a minimum thickness of 4 mm was enforced for the upper skin. On the lower skin, a minimum thickness of 20 mm was imposed in the pylon attachment area, with a 6 mm and 8 mm minimum thicknesses constraint outboard and inboard of this region.

### 3.7 Load Cases

Pull-up and push-over manoeuvres were defined to be structurally design driving. The MTOW configuration was used in the manoeuvres to generate the most critical aerostructural loads for the structural constraints. These load cases were trimmed to balance the pitching moment and ensure equilibrium between aerodynamic and inertial forces, with the angle of attack and elevator deflection serving as trimming variables. A summary of structurally design driving load cases is presented in Table 4.

The aerostructural analysis used to obtain the aerodynamic loads for the drag-dependent objectives (Section 2.2) was conducted under cruise conditions with the MZFW configu-

Table 4: Load cases considered in the structural optimisation.

| **Load case** | **Load factor [g]** | **Mach** | **Altitude [m]** |
|---|---|---|---|
| Pull-up | 2.5 | 0.81 | 11,000 |
| Push-over | -1 | | |

ration, at a Mach number of 0.78 and an altitude of 10,363 metres, corresponding to a Reynolds number of 22 million. The aircraft was trimmed to achieve a target lift force using a gradient-based approach with the angle of attack as the trimming variable.

## 4 RESULTS

Prior to the structural sizing optimisations, both F25-AR15 and F25-AR17 had generic uniform material thickness with an initial MTOW of 81,656 kg. As expected, neither variant satisfied the imposed criteria prior to structural sizing, with significant constraint violations, particularly near the wing root.

### 4.1 Structural Sizing For Mass Minimisation

Having infeasible baseline designs as a starting point, both the F25-AR15 and F25-AR17 underwent structural sizing for mass minimisation using the optimisation process depicted in Figure 1. The structural sizing reduced the maximum constraint violation by six orders of magnitude. Table 5 summarises the characteristics of interest for both variants following the convergence of the conventional structural sizing. The results of the F25-AR15 serve as reference for all following optimisations.

Table 5: Key characteristics of both variants after conventional structural sizing.

| | **F25-AR15** | **F25-AR17** |
|---|---|---|
| MTOW [kg] | 81,618 | 81,836 |
| Normed $L/D$ [-] | 1.0000 | 1.0216 |
| Normed root bending moment [-] | 1.0000 | 1.0597 |

The MTOW for the optimised F25-AR17 is 218 kg (0.27%) heavier than that of the F25-AR15. This difference can be attributed to the additional material required due to the 7.5% larger wing surface area of the F25-AR17, as well as the increased thickness of structural components at the wing root necessary due to the 5.97% higher bending moments associated with the increased aspect ratio. Compared to the initial MTOW, the mass gains may not appear significant, with the MTOW of the F25-AR17 even slightly heavier than its baseline configuration. However, the optimisation ensures a design that satisfies all imposed constraints, a condition not met by the initial configurations.

The F25-AR17 has a 2.16% higher aerodynamic efficiency, compared to the F25-AR15. This can be attributed to the reduction in drag associated with the higher aspect-ratio. In fact, even though the friction drag of the F25-AR17 is 4.43% higher than that of the F25-AR15, due to the higher aspect-ratio larger wetted wing area, its pressure drag decreased by 6.74%.

The structural sizing with mass minimisation as the objective has yielded feasible designs, which serve as the starting points for the subsequent two optimisation cases.

## 4.2 Structural Sizing For Aerodynamic Efficiency

Following the structural sizing for mass minimisation, two additional structural sizing optimisations with distinct objectives are conducted for each aspect ratio. The optimisation process illustrated in Figure 2, which integrates the aerostructural performance model outlined in Section 2.2 into the conventional structural sizing process, is used.

Aerodynamic efficiency is selected as one of the objective functions of interest to provide a contrast with the conventional structural sizing approach, which focuses on minimising structural mass. The convergence history for the structural sizing optimisations for aerodynamic efficiency is illustrated in Figure 11.

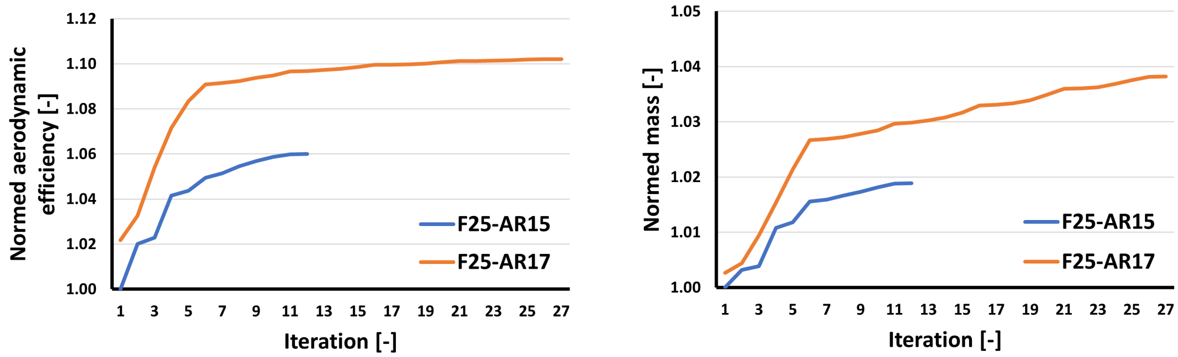


(a) Aerodynamic efficiency

(b) Aircraft MTOW

Figure 11: Convergence history of the structural sizing for aerodynamic efficiency.

Starting from the mass-optimal designs, the optimisations converge quickly and smoothly. However, only the final iterations yielded feasible designs.

The aerodynamic efficiency of the F25-AR15 increases 6.00%, albeit at the expense of a 1.89% increase in MTOW. Similarly, the F25-AR17 aerodynamic efficiency improved 7.86% at the cost of a 3.54% increase in MTOW, compared to its mass-optimal design. These results highlight the distinct design characteristics that emerge when aerodynamic efficiency is prioritised over structural weight.

The improvements in aerodynamic efficiency, relative to the conventional structural sizing, are due to a reduction in pressure drag. This reduction arises from a shift in the lift distribution, with the centre of lift moving outboard by more than 10%, as illustrated in Figure 13.

As a consequence of this shift, the wing root bending moment increases by more than 10%, directly affecting the mass. In the conventional structural sizing, minimising wing root bending moments through passive load alleviation is crucial for mass reduction, however, when the design objective shifts towards aerodynamic performance, this consideration is deprioritised.

When comparing the two aspect ratio configurations, the F25-AR17 exhibits a 3.98% higher aerodynamic efficiency due to its lower drag. This emphasises the potential of higher aspect-ratio wings to improve aerodynamic performance at the investigated conditions.

### 4.3 Structural Sizing For Breguet Range

Following the structural sizing optimisations for structural and aerodynamic performance metrics, Breguet range was selected as the final objective function. Breguet range is a comprehensive measure of overall aircraft performance, providing a trade-off between structural and aerodynamic efficiency in a physically meaningful manner. The Breguet range of the aircraft can be estimated for a simplified cruise segment as [35],

$$R_{Br} = \frac{aM}{\text{TSFC}} \frac{L}{D} \ln\left(\frac{W_{\text{initial}}}{W_{\text{final}}}\right), \tag{4}$$

where the Mach number $M$ and the speed of sound $a$ are functions of altitude and velocity; TSFC denotes the thrust-specific fuel consumption, which is determined by the propulsion system; the lift-to-drag ratio denotes the aerodynamic efficiency; and $W_{\text{initial}}$ and $W_{\text{final}}$ correspond to the total aircraft mass at the beginning and end of the cruise segment.

Figure 12 presents the convergence history for the structural sizing optimisation for Breguet range. The starting point for this optimisation was also the designs obtained from the conventional structural sizing.

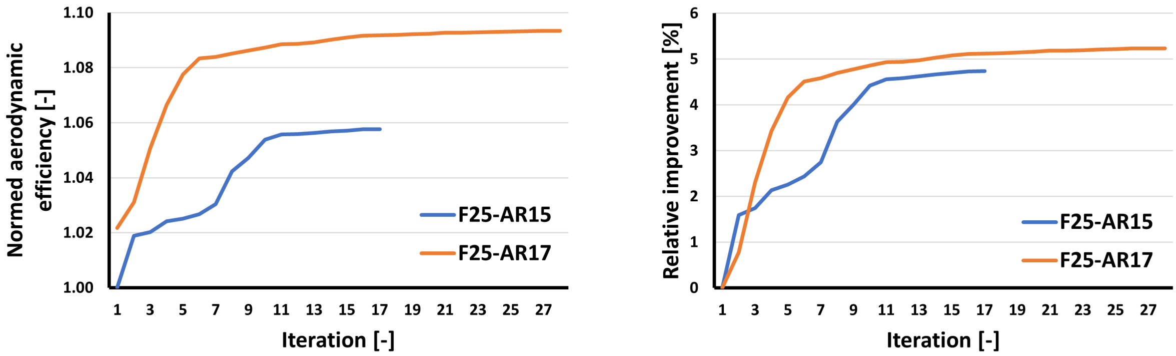


(a) Aerodynamic efficiency (b) Breguet range improvement

Figure 12: Convergence history of the structural sizing for Breguet range.

During the optimisations, the Breguet range improved by 4.73% and 5.23% for the F25-AR15 and F25-AR17, respectively. These optimised designs maintain an aerodynamic efficiency similar to that obtained for the $L/D$ objective, with only a marginal difference of 0.23% and 0.80%, while simultaneously achieving a substantial mass reduction of 0.94% and 1.89% for the F25-AR15 and F25-AR17, respectively. The final masses of the designs optimised for Breguet range are between those obtained through structural sizing for minimal mass and those derived from aerodynamic efficiency objectives. The wing root bending moments are very similar compared to the optimisations for aerodynamic efficiency, as a result of the near-identical lift distributions.

The drag reduction associated with the higher aspect-ratio wing is also observed in the optimisations for Breguet range. Despite having a greater wetted surface area, the F25-AR17 exhibits a 3.38% lower drag, highlighting the aerodynamic advantages conferred by the higher aspect ratio in this context.

The optimisations for Breguet range took longer to convergence compared to the aerodynamic efficiency objective, due to the conflicting nature of aerodynamic and structural performance. The average runtime per iteration for the primal solution was approximately

1 hour and 20 minutes, with approximately half of this time allocated to the loads model and the other half to the high-fidelity aerostructural analysis. The sensitivity analysis required approximately 2 hours per iteration, again with an even distribution between the loads and the performance analysis model.

Figure 13 illustrates the lift distributions after the structural sizing optimisations considering mass, aerodynamic efficiency, and Breguet range as objectives.

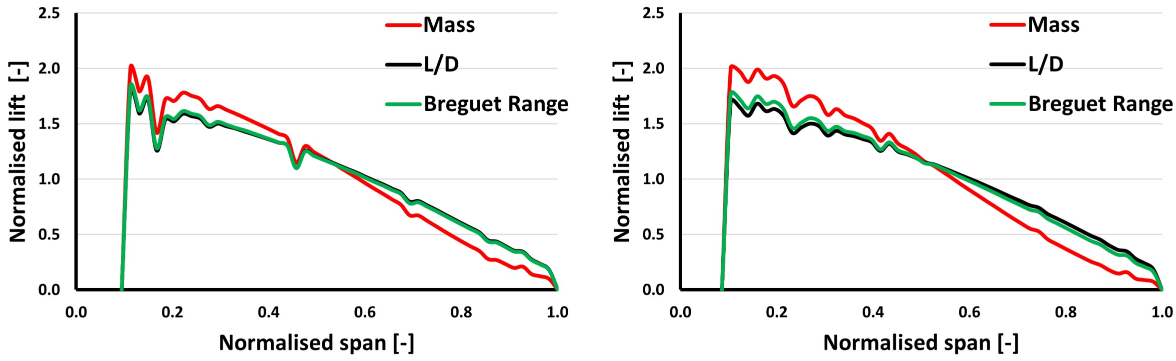


(a) F25-AR15 (b) F25-AR17

Figure 13: Lift distributions for the structural sizing optimisations for mass, aerodynamic efficiency, and Breguet range.

All optimisation cases exhibit lift distributions that closely resemble the bell-shaped distribution proposed by Prandtl in 1933 as the aerostructurally optimal lift distribution for wing designs with variable span and constant weight [36]. For both aspect ratios, the structural sizing optimisations aimed at reducing finite element mass shift the aerodynamic loads inboard to reduce the wing root bending moment, which is one of the main contributors to structural mass in wing design, through passive load alleviation. The optimisations for aerodynamic efficiency and Breguet range produce lift distributions that are very similar to each other and start tending towards an elliptical profile, highlighting the prioritisation of drag reduction in these objectives.

Figure 14 presents a comparison between the F25-AR15 and F25-AR17 Pareto fronts. These Pareto fronts were estimated based on the three optimal design points, corresponding to the minimisation of structural mass, maximisation of aerodynamic efficiency, and the optimisation of Breguet range.

When comparing the results of the first two optimisation cases, which focused on a single discipline objective, with those obtained by optimising for the Breguet range, it becomes evident that the latter achieves a better trade-off between structural and aerodynamic efficiency, thereby resulting in superior overall aircraft performance in the investigated design points.

The F25-AR15 and F25-AR17 offer markedly different characteristics in terms of mass and lift-to-drag ratio. For short-range missions, the F25-AR15 configuration is more favourable due to its lower structural weight. Conversely, for longer missions, the F25-AR17 offers superior performance as a result to its improved aerodynamic efficiency.

The optimisations presented in this work do not take into account constraints imposed by overall aircraft design or by disciplines beyond structural mechanics. Nonetheless, the results presented herein may serve as a valuable reference for aircraft designers in

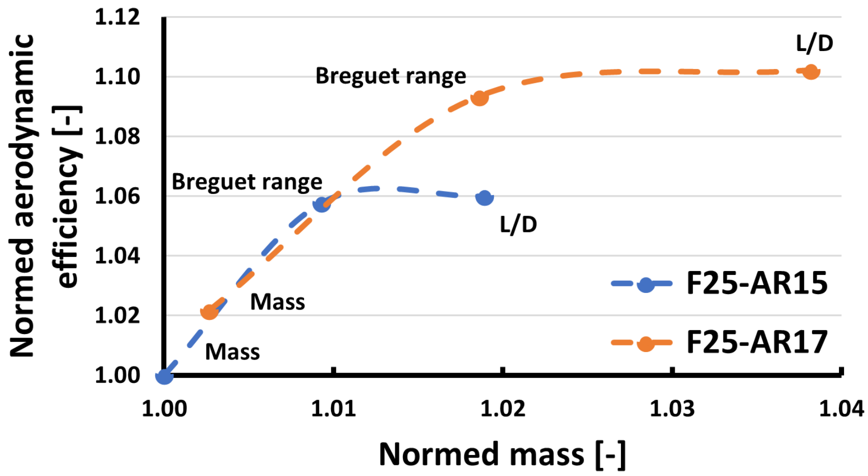


Figure 14: Pareto fronts for the F25-AR15 and F25-AR17.

informing the early stages of the design process.

## 5 CONCLUSIONS

This study investigated the aeroelastic structural sizing optimisation of two high aspect-ratio composite wings, using three distinct objective functions. The first two objectives -the minimisation of structural mass and the maximisation of aerodynamic efficiency - focused on a single discipline, whilst the third - the maximisation of the Breguet range - provided a multidisciplinary trade-off between the structural and aerodynamic domains. The optimisations were conducted using a high-fidelity multidisciplinary design optimisation framework, integrating DLR's CFD solver TAU and Airbus' structural solver Lagrange. A gradient-based algorithm with direct sensitivity analysis was used. The design variables, which are in the order of the 3,000, included structural sizing parameters, such as the thickness or cross-sectional area of the skin, spars, and stringers, while the constraints encompassed structural strength, buckling stability, and manufacturing criteria.

The results capture the effects of increasing the aspect ratio in modern transport aircraft, particularly the reduction in drag and consequent increase in aerodynamic efficiency, and the associated increase in structural weight. These findings may assist designers in evaluating the impact of aspect ratio on overall aircraft performance. Furthermore, the study demonstrates that using a multidisciplinary performance-based objective such as the Breguet range in the structural sizing optimisations during the preliminary design stage facilitates a trade-off between structural and aerodynamic efficiency.

Future work should expand the current shape parameter study to more aspect ratios, exploiting the opportunity to run these optimisations in parallel. Furthermore, shape variables, such as jig twist and aerofoil geometry, should be integrated into the design space. Moreover, a broader range of load cases, such as gust encounters and aeroelastic phenomena like flutter should be added to yield more realistic and robust design outcomes.

## ACKNOWLEDGEMENTS

The project Ultra Performance Wing (UP Wing, project number: 101101974) is supported by the Clean Aviation Joint Undertaking and its members. Co-Funded by the European Union. Views and opinions expressed are however those of the authors only and do not necessarily reflect those of the European Union or Clean Aviation Joint Undertaking. Neither the European Union nor the granting authority can be held responsible for them.

## REFERENCES

[1] Clean Aviation Joint Undertaking. Strategic Research and Innovation Agenda. Technical Report CAJU-GB-2021-12-16-SRIA, European Commision, December 2021.

[2] I. Kroo. Drag due to lift: concepts for prediction and reduction. *Annual review of fluid mechanics*, 33:587–617, 01 2001. doi:10.1146/annurev.fluid.33.1.587.

[3] F. Daoud, S. Deinert, R. Maierl, and Ö. Petersson. Integrated multidisciplinary aircraft design process supported by a decentral MDO framework. In *16th AIAA/ISSMO Multidisciplinary Analysis and Optimization Conference*, Dallas, Texas, June 2015. doi:10.2514/6.2015-3090.

[4] G. J. Kennedy and J. R. R. A. Martins. A Comparison of Metallic and Composite Aircraft Wings Using Aerostructural Design Optimization. In *14th AIAA/ISSMO Multidisciplinary Analysis and Optimization Conference*, Indianapolis, Indiana, September 2012. doi:10.2514/6.2012-5475.

[5] S. Wöhler, J. Häßy and V. Kriewall. Establishing the DLR-F25 as a research baseline aircraft for the short-medium range market in 2035. In *34th Congress of the International Council of the Aeronautical Sciences,*. Florence, Italy, September 2024.

[6] M. Schulze, F. Müller, S. Cumnuantip, V. Handojo, T. Hecken, T. Klimmek, M. Ritter, and M. Zimmer. The Effect of Aspect Ratio Variation on the Preliminary Aeroelastic Assessment of a Mid-Range Transport Aircraft. In *International Forum on Aeroelasticity and Structural Dynamics*, The Hague, Netherlands, June 2024.

[7] S. Deinert. *Shape and Sizing Optimization of Aircraft Structures with Aeroelastic and Induced Drag Requirements*. PhD thesis, Technische Universität München, 2016.

[8] A. B. Lambe and J. R. R. A. Martins. Extensions to the design structure matrix for the description of multidisciplinary design, analysis, and optimization processes. *Structural and Multidisciplinary Optimization*, 46:273–284, 2012. doi:10.1007/s00158-012-0763-y.

[9] F. Volle. Aero-Structural Optimization of the AIAA MDO Benchmark Model With TAU and Lagrange. In *AIAA SCITECH 2025 Forum*, Orlando, Florida, January 2025. doi:10.2514/6.2025-2815.

[10] F. Volle, M. Abu-Zurayk, A. U. Balani, S. Deinert and Ö. Petersson. Simultaneous Shape and Sizing Optimization for Improving Aircraft Performance Using the Aero-Structure Adjoint. In *Deutsche Luft- und Raumfahrtkongress - DLRK*, Stuttgart, Germany, September 2023.

[11] A. A. Gastaldi, F. Volle, F. Daoud, C. Breitsamter. Simultaneous Airframe Shape and Sizing Optimization Using FlowSimulator and the Lagrange MDO Suite. In *Deutsche Luft- und Raumfahrtkongress - DLRK*, Dresden, Germany, September 2022.

[12] G. Schuhmacher, F. Daoud, Ö. Petersson and M. Wagner. Multidisciplinary Airframe Design Optimization. In *28th International Congress of the Aeronautical Sciences*. Brisbane, Australia, September 2012.

[13] F. Daoud, Ö. Petersson, S. Deinert and P. Bronny. Multidisciplinary Airframe Design Process: Incorporation of steady and unsteady aeroelastic loads. In *12th AIAA Aviation Technology, Integration, and Operations (ATIO) Conference and 14th AIAA/ISSMO Multidisciplinary Analysis and Optimization Conferences*. Indianapolis, Indiana, September 2012.

[14] D. Schwamborn, T. Gerhold, R. Heinrich. The DLR TAU-code: recent applications in research and industry. In *ECCOMAS CFD Conference*, Delft, Netherlands, 2006.

[15] S. Langer, A. Schwöppe, and N. Kroll. The DLR Flow Solver TAU - Status and Recent Algorithmic Developments. In *52nd Aerospace Sciences Meeting*. Maryland, USA, January 2014.

[16] M. Meinel and G. Ó. Einarsson. The FlowSimulator framework for massively parallel CFD applications. In *Applied parallel and scientific computing 10th International Conference*. Reykjavik, Iceland, June 2010.

[17] U. Küttler and A. W. Wall. Fixed-point fluid-structure interaction solvers with dynamic relaxation. *Computational mechanics*, 43(1):61–72, 2008.

[18] E. Albano and W. P. Rodden. A doublet-lattice method for calculating lift distributions on oscillating surfaces in subsonic flows. *AIAA journal*, 7(2):279–285, 1969. doi:10.2514/3.5086.

[19] R. L. Harder and R. N. Desmarais. Interpolation using surface splines. *Journal of aircraft*, 9(2):189–191, 1972. doi:10.2514/3.44330.

[20] A. Schuster, L. Reimer and J. Neumann. A Mesh-Free Parallel Moving Least-Squares-based Interpolation Method for the Application in Aeroelastic Simulations With the Flow Simulator. *New Results in Numerical and Experimental Fluid Mechanics X*, 132:573–583, 2016. doi:10.1007/978-3-319-27279-5_50.

[21] A. Rempke. Netzdeformation mit Elastizitätsanalogie in multidisziplinärer FlowSimulator-Umgebung. In *Jahresbericht 2016 zum 20. DGLR-Fach-Symposium der STAB*. Braunschweig, Germany, November 2016.

[22] A. Eberle, B. Stefes, and D. Reckzeh. Clean Aviation Ultra-Performance Wing (UP-Wing). In *AIAA SCITECH 2024 Forum*, Orlando, Florida, January 2024. doi:doi.org/10.2514/6.2024-2109.

[23] Á. R. Triviño. Horizontal double bubble aircraft design for the middle of the market. Master's thesis, Universidad Europea De Madrid, 2024.

[24] Airbus. A321 aircraft characteristics - airport and maintenance planning. Technical report, Airbus S.A.S., 2005.

[25] C. M. Liersch and M. Hepperle. A distributed toolbox for multidisciplinary preliminary aircraft design. *CEAS Aeronautical Journal*, 2:57–68, 2011.

[26] B. Nagel, D. Böhnke, V. Gollnick, P. Schmollgruber, A. Rizzi, G. La Rocca, J. J. Alonso. Communication in aircraft design: Can we establish a common language. In *28th International Congress of the Aeronautical Sciences*. Brisbane, Australia, September 2012.

[27] R. Maierl, Ö. Petersson, F. Daoud. Automated Creation of Aeroelastic Optimization Models from a Parameterized Geometry. In *15th International Forum on Aeroelasticity and Structural Dynamics*, June 2013.

[28] S. Deinert, Ö. Petersson, F. Daoud and H. Baier. Aircraft loft optimization with respect to aeroelastic lift and induced drag loads. In *10th World Congress on Structural and Multidisciplinary Optimization*, May 2013.

[29] K. Schittkowski. NLPQL: A FORTRAN subroutine solving constrained nonlinear programming problems. *Annals of operations research*, 5:485–500, 1986. doi:10.1007/BF02022087.

[30] S. Boyd and L. Vandenberghe. *Convex optimization.* Cambridge university press, 2004.

[31] P. M. Weaver. On Optimisation of Long Anisotropic Flat Plates Subject to Shear Buckling Loads. In *45th AIAA/ASME/ASCE/AHS/ASC Structures, Structural Dynamics & Materials Conference*. Palm Springs, California, April 2004. doi:10.2514/6.2004-2053.

[32] P. M. Weaver. Design Formulae for Buckling of Biaxially Loaded Laminated Rectangular Plates with Flexural/twist Anisotropy. In *46th AIAA/ASME/ASCE/AHS/ASC Structures, Structural Dynamics and Materials Conference*. Austin, Texas, April 2005. doi:10.2514/6.2005-2105.

[33] P. M. Weaver. Approximate analysis for buckling of compression loaded long rectangular plates with flexural/twist anisotropy. *Proceedings of the Royal Society A: Mathematical, Physical and Engineering Sciences*, 462(2065):59–73, 2006. doi:10.1098/rspa.2005.1552.

[34] D. E. Calderon, J. E. Cooper, M. Lowenberg, S. A. Neild and E. B. Coetzee. Sizing High-Aspect-Ratio Wings with a Geometrically Nonlinear Beam Model. *Journal of Aircraf*, 56:1455–1470, 2019. doi:10.2514/1.C035296.

[35] D. Raymer. *Aircraft Design: A Conceptual Approach.* American Institute of Aeronautics and Astronautics, 2012. ISBN 0-930403-51-7. doi:10.2514/4.869112.

[36] L. Prandtl. Über Tragflügel kleinsten induzierten Widerstandes. In *Zeitschrift für Flugtechnik und Motorluftschiffahrt*, volume 24, pages 305–306, 1933.